Eur. Phys. J. B **3**, 1–5 (1998)

THE EUROPEAN PHYSICAL JOURNAL B

© EDP Sciences
Springer-Verlag 1998

Hydrogen storage in icosahedral and related phases of rapidly solidified Ti–Zr–Ni alloys

R. Nicula[1], A. Jianu[1], A.R. Biris[2], D. Lupu[2], R. Manaila[1], A. Devenyi[1], C. Kumpf[3,a], and E. Burkel[3]

[1] National Institute of Materials Physics, P.O. Box MG-7, 76900, Bucharest-Magurele, Romania
[2] ITIM-Cluj, Donath str. 65-103, 34600 Cluj-Napoca, Romania
[3] LS Physik Neuer Materialien, FB Physik, Universität Rostock, August-Bebel-Str. 55, 18051 Rostock, Germany

Received: 26 August 1997 / Revised: 8 January 1998 / Accepted: 10 February 1998

Abstract. High-resolution synchrotron-radiation powder diffraction experiments were performed to observe structural changes induced by hydrogen loading in rapidly-quenched Ti–Zr–Ni alloy ribbons with dominant icosahedral character. Lattice expansion effects due to hydrogen storage in Ti–Zr–Ni quasicrystals as well as phonon and phason disorder coefficients are obtained from an analysis of diffraction linewidths.

PACS. 61.44.Br Quasicrystals – 61.10.Nz Single-crystal and powder diffraction

1 Introduction

The icosahedral (ICO) phase and large unit-cell crystalline approximant (CA) structures frequently occur in rapidly solidified Ti-transition metal (TM) alloys, their presence being so far reported for Ti–TM (TM: Fe, Ni, Mn, Co) [1], Ti–TM–Si (TM: Cr, V) [2,3], Ti–TM–Ni (TM: Zr, V) [4,5] and several other alloy systems. Related crystalline phases having similar atomic clusters as elementary building blocks (hcp $MgZn_2$-type Laves, bcc β-Ti solid solution, fcc Ti_2Ni-type) strongly compete for formation with the ICO/CA phases in Ti-based alloys.

Hydrogen atoms preferentially occupy tetrahedrally-coordinated sites in most TM alloys [6]. Icosahedral alloys are also dominated by local tetrahedral order [7]. Titanium based ICO alloys are presently regarded as very promising hydrogen storage materials, mainly due to the expected high-density of sites available for interstitial H and to the favorable metal-hydrogen chemistry [8]. Among these, the Ti–Zr–Ni ICO-phases are known to exhibit a very high degree of icosahedral perfection and presumably the highest density of atomic sites with tetrahedral coordination. In addition, hydrogen has a high chemical affinity for both Ti and Zr, with which it forms a large number of compounds. In spite of the relative easiness with which the ICO-phase can be obtained as the major alloy component, rapidly-quenched Ti–Zr–Ni alloys are obtained in most cases as mixtures of ICO/CA and related crystalline phases [9]. Moreover, slightly different compositions and rapid solidification parameters lead to the formation of different phase mixtures. Because of the ability of these related phases to also store H in various amounts, an investigation of hydrogen absorption effects on sample morphology/structure may prove useful to the optimization of these materials with respect to hydrogen storage applications. We report on structure modifications induced by hydrogen loading in an ICO + hexagonal close-packed (hcp) Laves phase mixture, examined using synchrotron radiation high-resolution powder diffraction (HRPD).

2 Experimental

Primary alloy ingots were obtained from high-purity elements by arc-melting in water-cooled copper moulds. The ingots were further induction melted in fused-silica crucibles and rapidly quenched onto a copper wheel, in protective Ar atmosphere. Quenching linear speeds of 20 and 25 m/s were used to obtain ribbons 1-10 cm long with an average cross-sectional area of 1.5 mm $\times$ 45 μm. Icosahedral phase formation was initially assesed by conventional X-ray diffraction using CuK_α radiation.

The morphology and local composition of the as-quenched ribbons were examined by transmission electron microscopy (TEM, Philips CM30) and energy dispersive spectroscopy (EDS). EDS analysis revealed no signs of Si contamination. Nevertheless, Si content of up to about 2 at.% is rather difficult to rule out.

As-quenched $Ti_{41.5}Zr_{42.3}Ni_{16.2}$ ribbons were submitted to hydrogenation from the gas phase, using the Sieverts method [10]. Impurification from the reactor walls was prevented by degassing the reaction vessel at 300 °C for 3 hours. The ribbons were then exposed to ultra-high purity (99.9999%) hydrogen gas in the constant volume reactor at 300 °C and 30 bar hydrogen pressure. Since

[a] *Present address:* LS Kristallographie, Institut für Angewandte Physik, Universität Erlangen-Nürnberg, Bismarckstr. 10, 91054 Erlangen, Germany. e-mail: kumpf@desy.de

Ti- and Zr-based Laves phases are known to posess rather active surfaces and are less sensitive to the presence of surface oxygen [11], no measures were taken to speed up the activation process. The observed induction period was about 20 hours. The amount of hydrogen taken up by the $Ti_{41.5}Zr_{42.3}Ni_{16.2}$ samples was followed by measuring the pressure drop (typically around 5 bar) in the sealed reactor chamber. The equilibrium plateau pressure $P_{eq} = 25$ bar was reached after about 100 hours. After hydrogenation, the reactor was rapidly cooled down to room temperature and hydrogen loss during later sample handling was prevented by the adsorption of a thin CO surface layer [11]. The highest total hydrogen loading capacity of the $Ti_{41.5}Zr_{42.3}Ni_{16.2}$ samples was H/M = 1.5, higher than the H/M value of the $LaNi_5$ compound used for most hydride batteries today [12].

As-quenched and hydrogenated $Ti_{41.5}Zr_{42.3}Ni_{16.2}$ ribbons were studied by HRPD [13] at the B2 beamline of the Deutsches Elektronen Synchrotron DESY/HASYLAB (Hamburg, Germany). The radiation source at this beamline is a bending magnet with a critical energy $E_c = 16.6$ keV. A gold-coated toroidal focusing mirror is placed in front of the double-crystal Ge(111) monochromator. The primary intensity is monitored by a gas-ionisation chamber. In focused beam mode, the incoming monochromatic beam provides $10^8 - 10^9$ photons/s. A Ge(111) analyser crystal is placed in the diffracted beam, in front of the NaI scintillation counter. Each diffraction pattern was recorded at constant monitor rate (6000 counts/point), within step-scanning mode single runs. The patterns were measured using a constant angular step $\Delta 2\theta = 0.01°$ and synchrotron radiation wavelength $\lambda = 1.29$ Å. Wavelength calibration was performed several times between the measurements, using standard Si powder samples. For the present diffraction experiments the Q-resolution was $\Delta Q \leq 5.24 \times 10^{-2}$ Å^{-1} ($4\pi \sin\theta/\lambda$ units).

The high energy-resolution conditions enabled efficient removal of the inelastic scattering component from the diffraction patterns. An abundance of low-intensity peaks was thus revealed, as expected for icosahedral structures. Peak positions and linewidths were further evaluated by profile matching with Voigt functions. Lattice parameters were derived by extrapolation *versus* $\cos^2\theta$, $\mathrm{cotan}^2\theta$ and $\cos\theta \mathrm{cotan}\,\theta$, which yield the best linear correlation of instrumental errors on line positions. The ICO-phase was indexed according to the scheme proposed by Cahn *et al.* [14], using (N, M) indices. Positions of icosahedral lines (centroids) were used to derive the extrapolated a_{6D} parameter of the hypercubic 6D lattice using:

$$Q_{par} = \frac{2\pi}{a_{6D}} \sqrt{\frac{N + M\tau}{2(2+\tau)}} \qquad (1)$$

where $Q_{par} \equiv 4\pi \sin\theta/\lambda$ is the physical (parallel) component of the 6D scattering vector. The complementary (Q_{perp}) component of the 6D scattering vector is then:

$$Q_{perp} = \frac{2\pi}{a_{6D}} \sqrt{\frac{\tau(N\tau - M)}{2(2+\tau)}}\,. \qquad (2)$$

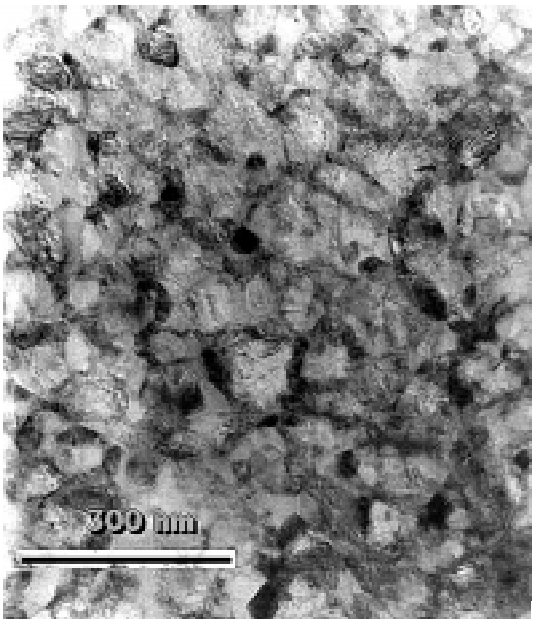

Fig. 1. Bright-field TEM micrograph of non-hydrogenated $Ti_{41.5}Zr_{42.3}Ni_{16.2}$ as-quenched ribbons, showing a fine mixture of icosahedral and hcp Laves grains. Moiré fringes indicate that the two phases are structurally related, mainly through orientational correlations.

The 3D quasilattice parameter $a_q \equiv \frac{a_{6D}}{\sqrt{2}}$ of the ICO-phase was alternatively determined using a least-squares procedure providing the best fit to the observed positions of the ICO lines. The differences between the a_{6D} values obtained using the above extrapolation functions or the least-squares procedure were within experimental errors.

3 Results and discussion

3.1 Microstructure

Bright-field TEM micrographs of the non-hydrogenated $Ti_{41.5}Zr_{42.3}Ni_{16.2}$ ribbons (Fig. 1) reveal a nanometer-sized mixture of ICO and hcp Laves grains. Regions of dominant ICO-phase and dominant Laves phase respectively, could be identified. This is to be considered an effect of slightly different solidification conditions in various parts of the sample.

Moiré fringes can also be noticed in the bright-field electron micrographs of non-hydrogenated $Ti_{41.5}Zr_{42.3}Ni_{16.2}$ ribbons. Such fringes usually occur if overlapping crystals with almost exactly equal or multiple interplanar spacings are imaged by combining the transmitted beam and the double diffracted spots [15]. The observed Moiré patterns indicate the presence of two or more structurally related phases and are probably due to the orientational relationship between these.

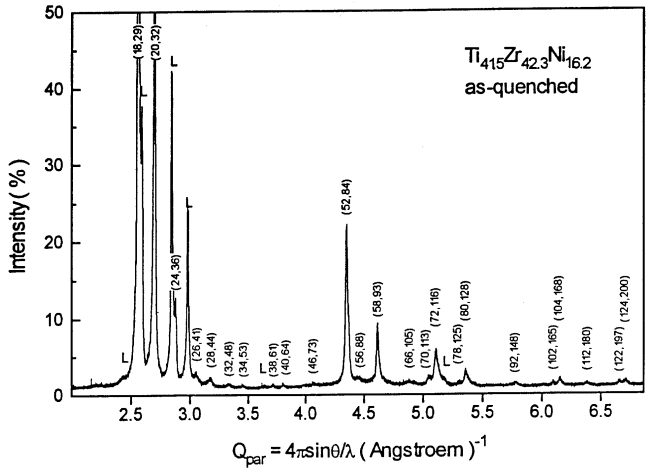

Fig. 2. High-resolution powder diffraction pattern of as-quenched non-hydrogenated $Ti_{41.5}Zr_{42.3}Ni_{16.2}$ ribbons. ICO-phase lines are indexed with (N, M) Cahn indices. Symbol L denotes diffraction lines of the hcp Laves phase.

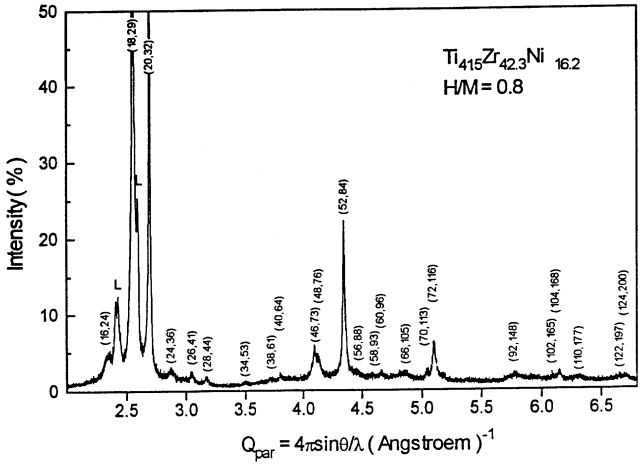

Fig. 3. High-resolution powder diffraction pattern of hydrogenated $Ti_{41.5}Zr_{42.3}Ni_{16.2}$ ribbons, H/M = 0.8.

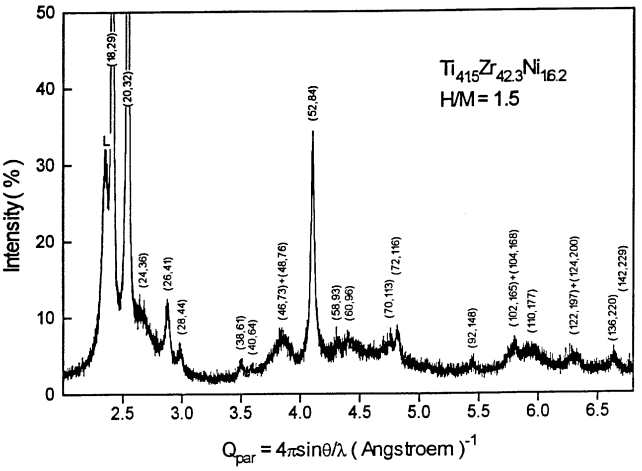

Fig. 4. High-resolution powder diffraction pattern of hydrogenated $Ti_{41.5}Zr_{42.3}Ni_{16.2}$ ribbons, H/M = 1.5.

3.2 Synchrotron radiation diffraction

For cooling speeds below 25 m/s, the icosahedral phase formation is strongly dependent on composition. Ribbons with composition $Ti_{67.1}Zr_{14.4}Ni_{18.5}$ consist of a nearly single-phase bcc β-Ti(ZrNi) solid solution. The lattice constant of this bcc phase was evaluated at $a = 3.31 \pm 0.001$ Å, in close agreement with the value reported for β-Ti, the high-temperature phase of titanium [16]. For cooling speeds equal or higher than 25 m/s, most as-quenched ribbons are either amorphous or consist of icosahedral grains embedded in an amorphous matrix.

The hydrogenation behaviour of rapidly-quenched $Ti_{41.5}Zr_{42.3}Ni_{16.2}$ alloy ribbons was investigated in more detail. The diffraction pattern of non-hydrogenated $Ti_{41.5}Zr_{42.3}Ni_{16.2}$ samples (Fig. 2) shows a dominant ICO-phase and a minor crystalline one. The latter is of the $MgZn_2$-type (C14, hcp Laves). Differential scanning calorimetry (DSC) studies [17] have shown that the ICO-phase crystallizes to this structure at around 700 °C. Only few diffraction lines of the Laves phase are free from superposition with peaks belonging to the major ICO-phase, leading to a less accurate evaluation of the hcp lattice parameters. These few accessible line positions of the Laves phase yielded lattice parameters $a = 5.08$ Å and $c = 8.68 \pm 0.01$ Å, which should be compared to $a = 5.18$ Å and $c = 8.52$ Å ($MgZn_2$), respectively $a = 5.064$ Å and $c = 8.21$ Å ($TiZn_2$) [16]. All of the remaining diffraction lines in the HRPD pattern could be unambiguously attributed to a primitive (P-type) hypercubic lattice of the ICO-phase. The ICO-phase quasilattice parameter was evaluated at $a_q = 5.21 \pm 0.003$ Å, corresponding to a 6D hypercubic lattice parameter $a_{6D} = 7.368$ Å. The a_q value is to be contrasted with the smaller $a_q = 5.12$ Å [4], 5.18 Å [8] and 5.19 Å [18] reported in the literature. This somewhat higher a_q value might be due to unwanted small-amount absorption of gas (O, N) atoms during the preparation process.

The hydrogenation process typically converts the ribbons into a gray-black powder. It is expected that hydrogen chemosorption induces lattice expansion effects, causing line broadening and peak shifting towards lower angles in the powder diffraction patterns. The HRPD patterns of hydrogenated $Ti_{41.5}Zr_{42.3}Ni_{16.2}$ ribbons with hydrogen/metal (H/M) atom ratios of 0.8 (Fig. 3) and 1.5 (Fig. 4) also reveal the presence of a prevalent ICO-phase.

For H/M = 0.8, the ICO-phase quasilattice parameter is equal to the one for the non-hydrogenated samples ($a_q = 5.21$ Å). Instead, the hcp $MgZn_2$-type Laves phase exhibits an increase of the lattice parameters to $a = 5.90$ Å and $c = 9.01 \pm 0.01$ Å. For H/M = 1.5, the lattice parameters of the hcp Laves phase maintain their increasing tendency ($a = 6.43$ Å and $c = 9.65 \pm 0.01$ Å), while H absorption in the ICO-phase becomes apparent through a 6% increase in the quasilattice parameter ($a_q = 5.52 \pm 0.005$ Å, $a_{6D} = 7.8065$ Å). The considerable increase in the diffuse scattering component of the three HRPD patterns should be correlated with the increasing hydrogen content.

3.3 Phonon and phason disorder

The instrumental FWHM was determined using standard Si powder samples. Values of the instrumental width b for particular scattering angles were obtained by interpolation. Corrected FWHM values B were obtained from experimental raw widths B_0 according to:

$$B^2 = (B_0 - b)(B_0^2 - b^2)^{1/2}. \quad (3)$$

Equation (3) is adequate for intermediate Gauss-Cauchy profiles [19]. Plotting B^2 *versus* Q_{par}^2 does not reveal any clear increasing dependence, as would be expected if the main source of line broadening were elastic strains caused by crystalline inclusions and/or inhomogeneous distortions [20].

FWHM's of icosahedral lines (B) were further used to assess the degree of random phason and phonon disorder by the relationship [19]:

$$B^2 = AQ_{par}^2 + CQ_{perp}^2. \quad (4)$$

The parameters measuring the degree of phonon (A) and random phason (C) disorder are determined by a fit to equation (4). The ratio of the two disorder parameters may then be used to asess the prevalence of a certain type of disorder over the other. Weak ICO peaks and ones affected by large superposition with hcp Laves diffraction lines were excluded from fitting equation (4) to corrected linewidths.

The evolution of phonon/phason disorder coefficients and quasilattice parameter with increasing H/M ratio is depicted in Figure 5. First, irrespective of the H/M value, the random phason disorder is at least one order of magnitude higher than the phonon disorder term, as noticed already for several Al-based quasicrystalline phases [19,21].

When loading the as-quenched ribbons up to a medium level H/M = 0.8, the phonon disorder coefficient A as well as the quasilattice parameter a_q are seen to remain unaffected, while a significant increase of the random phason coefficient C occurs. This is to be contrasted with the opposite behaviour of the hcp Laves phase, whose lattice parameters change considerably. The observed behaviour of the ICO-phase may be explained through the well-known ability of the icosahedral phase to acccomodate strains without apparent structural modifications. This very special property of the icosahedral phases comes from the fact that rearrangements of the ICO structure (involving displacements of larger groups of atoms or clusters) can take place at reduced energy costs. The process may nevertheless result in an increase in the degree of phason disorder.

At the highest loading levels attained (H/M = 1.5), the phason disorder coefficient C does not significantly change, indicating that the phason-based strain-compensation mechanism stabilizes. At this loading level, the hydrogen storage induced expansion effects affecting the icosahedral phase are detected mainly in physical (parallel) space through the increase of both quasilattice parameter and phonon disorder coefficient.

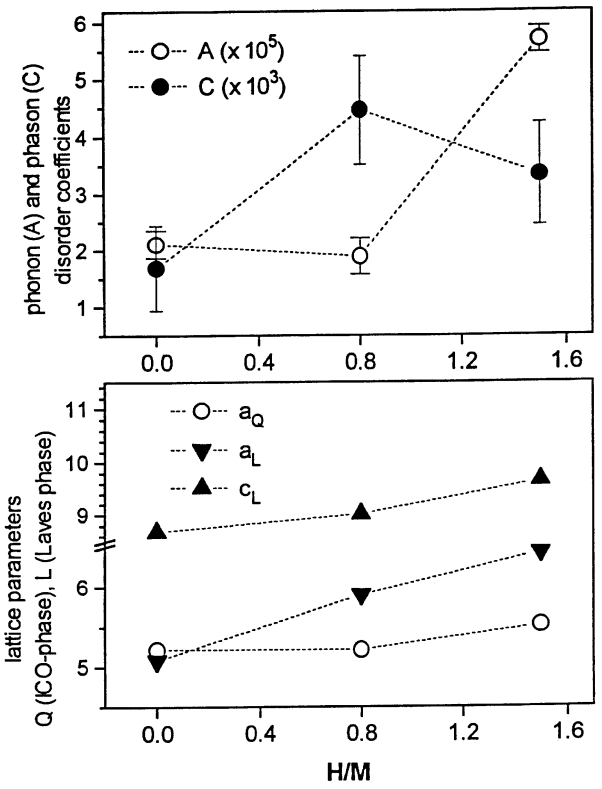

Fig. 5. Evolution of lattice parameters and disorder coefficients with hydrogen content H/M. The scaling factors are 10^5 for the phonon disorder coefficient (A) and 10^3 for the phason (C) disorder coefficient. Dotted lines are guides to the eye.

4 Concluding remarks

The formation of the ICO-phase in Ti–Zr–Ni alloys was found to be strongly dependent on alloy composition and rapid-quenching parameters. The ICO/CA and other related crystalline phases presumably attain stability at similar energies, so that fine-grained mixtures of crystalline and icosahedral phases are commonly obtained by rapid solidification.

High energy-resolution diffraction experiments using high-intensity synchrotron radiation allow for the evaluation of phonon/phason disorder coefficients of as-quenched and hydrogenated Ti–Zr–Ni alloys posessing dominant icosahedral character. It is suggested that moderate strains generated by hydrogen absorption are accomodated by the icosahedral structure at the cost of increasing phason disorder only, both quasilattice parameter and phonon disorder coefficient being unaffected. At higher H/M values, the effects are to be seen mainly in physical space, the random phason disorder coefficient maintaining a quasi-constant value.

One of the authors (R.N.) gratefully acknowledges financial support from the University of Rostock, the Synchrotron Radiation Laboratory DESY/HASYLAB (Hamburg) and the Deutscher Akademischer Austauschdienst (DAAD).

References

1. K.F. Kelton, P.C. Gibbons, P.H. Sabes, Phys. Rev. Lett. **38**, 7810 (1988).
2. X. Zhang, K.F. Kelton, Philos. Mag. Lett. **62**, 265 (1990).
3. X. Zhang, K.F. Kelton, Philos. Mag. Lett. **63**, 39 (1991).
4. X. Zhang, R.M. Stroud, J.L. Libbert, K.F. Kelton, Philos. Mag. B **70**, 927 (1994).
5. Z. Zhang, H.Q. Ye, K.H. Kuo, Philos. Mag. A **52**, L49 (1985).
6. C.S. Barett, T.B. Massalski, *Structure of Metals* (McGraw-Hill, New York, 1966).
7. D.R. Nelson, F. Spaepen, Solid State Phys. **42**, 1 (1989).
8. A.M. Viano, R.M. Stroud, P.C. Gibbons, A.F. McDowell, M.S. Conradi, K.F. Kelton, Phys. Rev. B **51**, 12026 (1995).
9. R.M. Stroud, K.F. Kelton, S.T. Misture, J. Mater. Res. **12**, 434 (1997).
10. J.P. Blackledge, *Metal Hydrides* (Academic Press, London, New York, 1968).
11. A. Percheron-Guegan, J.-M. Welter, *Hydrogen in Intermetallic Compounds I* (Springer, Berlin, Heidelberg, New-York, 1988).
12. K.F. Kelton, P.C. Gibbons, MRS Bull. **22/11**, 69 (1997).
13. R. Nicula, C. Kumpf, E. Burkel, DESY/HASYLAB Annual Report, vol. I, p. 598 (1996).
14. J.W. Cahn, D. Shechtman, D. Gratias, J. Mater. Res. **1**, 13 (1986).
15. J.W. Edington, *Practical Electron Microscopy in Materials Science* (London: Macmillan, 1975).
16. W.B. Pearson, *Handbook of lattice spacings and structures of metals and alloys* (Oxford: Pergamon Press, 1967).
17. R.M. Stroud, K.F. Kelton, in *Quasicrystals* (World Scientific Publishing Singapore, 1995).
18. A.M. Viano, A.F. McDowell, M.S. Conradi, R.M. Stroud, P.C. Gibbons, K.F. Kelton, in *Quasicrystals* (World Scientific Publishing Singapore, 1995).
19. Y. Calvayrac, A. Quivy, M. Bessiere, S. Lefebvre, M. Cornier-Quinquandon, D. Gratias, J. Phys. France **51**, 417 (1990).
20. P.M. Horn, W. Malzfeldt, D.P. DiVincenzo, J. Toner, R. Gambino, Phys. Rev. Lett. **57**, 1444 (1986).
21. R. Popescu, A. Jianu, M. Manciu, R. Nicula, R. Manaila, J. Alloys Compounds **221**, 240 (1995).